

X-ray-Controlled Bilayer Permeability of Bionic Nanocapsules Stabilized by Nucleobase Pairing Interactions for Pulsatile Drug Delivery

Hongzhang Deng, Lisen Lin, Sheng Wang, Guocan Yu, Zijian Zhou, Yijing Liu, Gang Niu, Jibin Song,* and Xiaoyuan Chen*

The targeted and sustained drug release from stimuli-responsive nanodelivery systems is limited by the irreversible and uncontrolled disruption of the currently used nanostructures. Bionic nanocapsules are designed by cross-linking polythymine and photoisomerized polyazobenzene (PETAzo) with adenine-modified ZnS (ZnS-A) nanoparticles (NPs) via nucleobase pairing. The ZnS-A NPs convert X-rays into UV radiation that isomerizes the azobenzene groups, which allows controlled diffusion of the active payloads across the bilayer membranes. In addition, the nucleobase pairing interactions between PETAzo and ZnS-A prevent drug leakage during their in vivo circulation, which not only enhances tumor accumulation but also maintains stability. These nanocapsules with tunable permeability show prolonged retention, remotely controlled drug release, enhanced targeted accumulation, and effective antitumor effects, indicating their potential as an anticancer drug delivery system.

Cellular organelles are compartmentalized by bilayer phospholipid membranes that allow the exchange of selective biomolecules and intercellular communication.^[1] Accordingly, various artificial self-assembled nanostructures with selective membrane permeation abilities have been explored as drug delivery systems to accelerate drug release in response to specific stimuli (e.g., pH, temperature, glucose, etc.).^[2] However, due to the irreversible dissociation of these nanostructures in response to the stimuli, drug release often cannot be controlled. In addition, the different tumor cells vary in their response to these drug delivery systems, which can lead to the accumulation

of sub-therapeutic levels at the targeting site, and thus reduce the efficacy of cancer chemotherapy.^[3] Therefore, it is essential to design nanostructures that enable controlled diffusion of the drugs across cellular membranes while maintaining their stability, in order to achieve targeted drug delivery and precise anticancer therapy. Layer-by-layer capsules, polymersomes, and polyion complex membrane have been successfully developed in recent years to address this issue.^[4] Polymersomes can be endowed with tunable permeability by simply integrating the stimuli-responsive moieties into their bilayer membranes. In addition, incorporation of light sensitive compounds into their shells allows remotely controlled and precise wavelength-dependent permeability switch.^[5]

Azobenzene is a class of photoswitchable compounds that were used for drug nanocarriers,^[6] optical/electrical switches,^[7] lithography,^[8] magnetic memories,^[9] and solar energy storage.^[10] It can be reversibly interconverted between the *trans* and *cis* isomeric forms upon UV, visible, or blue light irradiation.^[11] Although light-controlled drug delivery systems are noninvasive and have high localized targeting abilities, they require high-energy UV stimulation that severely limits their in vivo applications.^[12] UV light also has poor penetrative power due to absorption by the skin and underlying fat tissues,^[13] resulting in decreased photoconversion and drug release efficiency, and also induces direct tissue damage.^[14] In addition, the upconverting nanoparticles typically have low conversion efficiency that also limits UV application. To obviate these limitations, scintillating nanoparticles that emit photons in the visible and UV region upon X-ray irradiation have been developed.^[15] However, phototriggered isomerization of azobenzene is accompanied by microstructural rearrangement and irreversible nanocapsule disruption.^[16] Although chemical cross-linking can improve the structural stability, it can limit the permeability of hydrophilic and hydrophobic substances. Therefore, structures that allow controlled diffusion of active payloads while maintaining structural integrity are required. The natural base pairing between thymine (T) and adenine (A) via multiple hydrogen bonding has been translated into biomimetic structures, and is an attractive option for designing photostimulated nanocarriers.

Dr. H. Deng, Prof. J. Song
MOE Key Laboratory for Analytical Science of Food Safety and Biology
College of Chemistry
Fuzhou University
Fuzhou 350108, China
E-mail: jibinsong@fzu.edu.cn

Dr. H. Deng, Dr. L. Lin, Dr. S. Wang, Dr. G. Yu, Dr. Z. Zhou, Dr. Y. Liu,
Dr. G. Niu, Prof. X. Chen
Laboratory of Molecular Imaging and Nanomedicine (LOMIN)
National Institute of Biomedical Imaging and Bioengineering (NIBIB)
National Institutes of Health (NIH)
Bethesda, MD 20892, USA
E-mail: shawn.chen@nih.gov

 The ORCID identification number(s) for the author(s) of this article can be found under <https://doi.org/10.1002/adma.201903443>.

DOI: 10.1002/adma.201903443

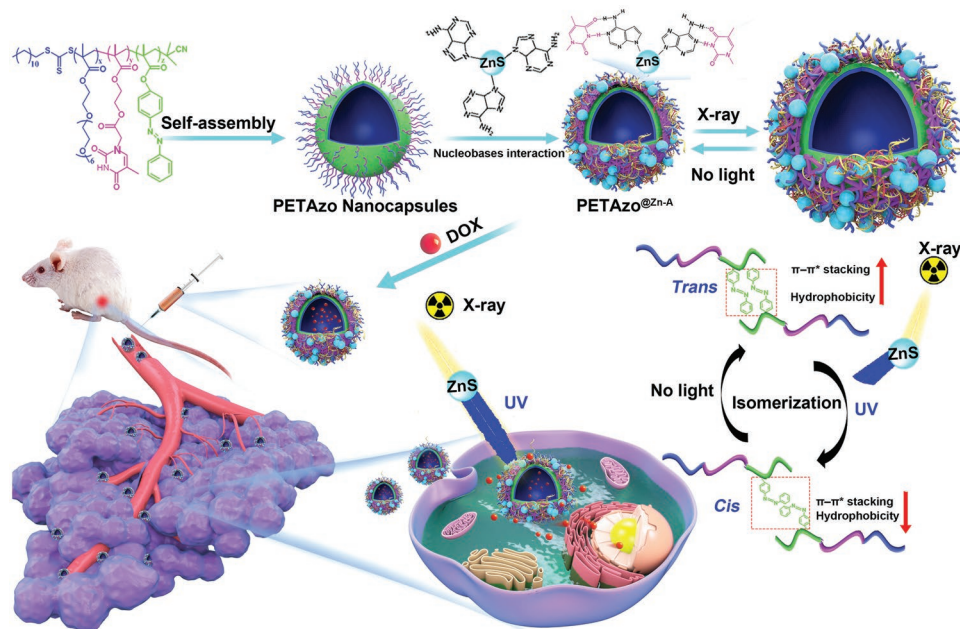


Figure 1. Schematic illustration of the self-assembly of poly(ethylene glycol)-*b*-polythymine-*b*-polyazobenzene (PETAzO) three-block polymers into nanocapsules with reversible photoinduced isomerization of azobenzene groups confined in the bilayer membrane at the interface of nanocapsules. The nanocapsules were cross-linked by nucleobase pairing interaction between PETAzO and adenine modified zinc sulfide nanoparticles (ZnS NPs), which is helpful to maintain the nanocapsules' structural stability before and after permeability switching. Scintillating ZnS NPs serve as the energy transducer to convert the highly penetrating X-rays into UV–vis light. The reversible photoisomerization (*trans* to *cis*) of the azobenzene group in the bilayer membrane of nanocapsules stimulated by UV light, which was transformed from X-ray irradiation, decreases the π – π^* stacking between azobenzene groups and hydrophobicity of azobenzene and induces the swelling of nanocapsules from initial 100 to 300 nm. The swelling of the nanocapsules prolongs the retention of the nanocapsules at the tumor site.

We fabricated X-ray-responsive bionic nanocapsules with reversible and tunable permeability by cross-linking the self-assembled triblock polymer poly(ethylene glycol)-*b*-polythymine-*b*-polyazobenzene (PETAzO) with adenine-modified zinc sulfide nanoparticles (ZnS-A NPs) through nucleobase pairing (Figure 1). While the PETAzO polymer provides the framework of the PETAzO@ZnS-A nanocapsules, the photoresponsive azobenzene residues control bilayer permeability, and the ZnS-A NPs convert X-rays into UV light to induce azobenzene isomerization and cross-link PETAzO and ZnS-A. Unlike other polymer capsule membranes that cannot switch back to the initial state after releasing the encapsulated cargo,^[16,17] PETAzO@ZnS-A nanocapsules maintain their mechanical integrity after selective payload diffusion owing to this cross-linkage. X-ray-mediated photoisomerization of the azo group also decreases the π – π^* stacking interactions between the azobenzene rings, which reduces hydrophobicity, induces nanocapsule swelling, and increases bilayer permeability.

The first step in fabricating PETAzO was the synthesis and purification of the carboxyl group-functionalized nucleobases (3-(9-adeninyl)-propionic acid (A-COOH) and 1-(carboxymethyl)thymine (T-COOH))^[18] (Figures S1–S5, Supporting Information), followed by preparation of 4-methacryloyloxyazobenzene and its characterization using nuclear magnetic resonance (NMR), liquid chromatography-mass spectrometry, high performance liquid chromatography, and gas chromatography-mass spectrometry (Figures S6–S11, Supporting Information). Poly(ethylene glycol)-*b*-polyhydroxyethyl

methacrylate-*b*-polyazobenzene was synthesized by reversible addition–fragmentation chain transfer polymerization (RAFT) of poly(ethylene glycol) methyl ether methacrylate, polyhydroxyethyl methacrylate, and 4-methacryloyloxyazobenzene with cyanomethyl dodecyl trithiocarbonate as the RAFT agent (Figures S12–S14, Supporting Information). The PETAzO three-block polymers were synthesized by esterification of poly(ethylene glycol)-*b*-polyhydroxyethyl methacrylate-*b*-polyazobenzene with T-COOH in the presence of *N,N*-dicyclohexylcarbodiimide/1,3-dicyclohexylcarbodiimide-4-dimethylaminopyridine (Figure S15, Supporting Information). The ¹H-NMR Mn values of the PETAzO polymer were consistent with the established theoretical values. A-COOH modified ZnS NPs (ZnS-A) were prepared as previously described,^[19] and transmission electron microscopy (TEM) images indicated that their average diameter was 8 nm (Figure 2a). High resolution TEM images revealed the high crystalline nature of ZnS-A NPs (Figure S16, Supporting Information). The selected area electron diffraction (SAED) pattern of ZnS-A exhibited the diffraction peaks assigned to the structure of ZnS (Figure S17, Supporting Information). The X-ray diffraction analysis of ZnS-A NPs (Figure S18, Supporting Information) indicated the three diffraction features appearing at about 28.8°, 47.9°, and 56.3° that correspond to the (111), (220), and (311) planes of the zinc blende phase of ZnS-A, respectively. Taken together, the ZnS nanoparticles were successfully constructed. The nanocapsules of PETAzO were prepared by the double emulsion solvent evaporation method (Figure 2b). To determine if the polythymine segments were on

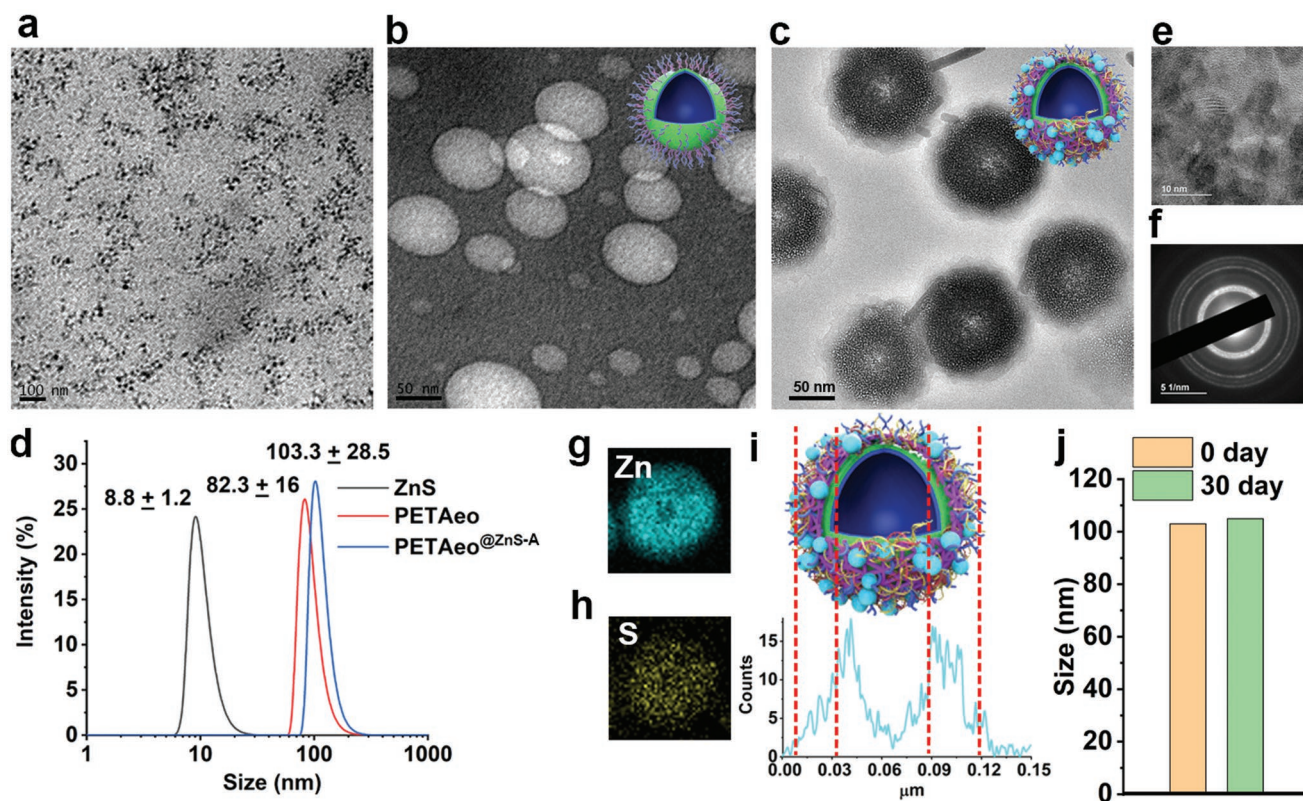


Figure 2. Nucleobase pairing fabrication and characterization of the nanocapsules. a–c) TEM images of ZnS-A nanoparticles (a), PETAzo nanocapsules (b), and PETAzo@ZnS-A nanocapsules (c). d) Hydrodynamic size distribution histograms of ZnS NPs, PETAzo, and PETAzo@ZnS-A nanocapsules. e) High-resolution TEM image of the shell of PETAzo@ZnS-A nanocapsules. f) Selected-area electron diffraction (SAED) of PETAzo@ZnS-A. g,h) Elemental mapping of Zn (g) and S (h). i) STEM electron energy-loss spectroscopy (STEM-EELS) line scan graph across a PETAzo@ZnS-A nanocapsule. j) Size variation of PETAzo@ZnS-A before and after 30 days incubation.

the surface of these nanocapsules, they were dispersed in D₂O and analyzed by ¹H NMR. While thymine signals were clearly seen, that of the hydrophobic blocks were weak, since these nanocapsules trap protons in their hydrophobic core which is shielded by the poly(ethylene glycol) (PEG) shell (Figure S19, Supporting Information). The PETAzo@ZnS-A nanocapsules were finally prepared by adding the ZnS-A NPs to a solution of PETAzo nanocapsules in PBS with constant stirring (Figure 2c). ¹H NMR showed a distinct contrast between the outer shell and core indicating the characteristic nanocapsule morphology (Figure 2b,c). In addition, the sizes of the PETAzo and PETAzo@ZnS-A nanocapsules were determined using laser particles size analyzer, and showed a slight increase in the average diameter of PETAzo with the incorporation of ZnS-A NPs from 80 to 100 nm (Figure 2d). High resolution TEM images revealed the highly crystalline nature of ZnS-A NPs (Figure 2e), and the SAED pattern confirmed that the ZnS-A NPs were tethered on the PETAzo nanocapsule bilayer by nucleobase pairing (Figure 2f). The surface localization of the ZnS-A NPs on the PETAzo nanocapsules was validated using high-angle annular dark-field scanning TEM (STEM) (Figure 2g,h), and STEM electron energy loss spectroscopy (STEM-EELS) line scanning analysis (Figure 2i). The size of PETAzo@ZnS-A nanocapsules did not significantly change after 30 days incubation in 10% fetal bovine serum (FBS) at 37 °C (Figure 2j), indicating PETAzo@ZnS-A has

high stability. Furthermore, to further prove the stability of the nanoparticles in serum, albumin from bovine serum (BSA) was used as a model protein to simulate the nonspecific protein adsorption under simulated physiological condition (pH 7.4). PETAzo@ZnS-A showed prominent monomer band similar to free BSA, indicating little BSA adsorption (Figure S20, Supporting Information). After incubation of PETAzo@ZnS-A with BSA for 12, 24, 48, 72, and 96 h, respectively, the mixed solution was centrifuged and the supernatant was collected. There was negligible amount of unadsorbed BSA in the supernatant (Figure S21, Supporting Information). This result also indicated high stability of PETAzo@ZnS-A. The loading content and efficiency of the nanocapsules were 12.1% and 75%, respectively (Table S1, Supporting Information), and increased with increasing concentration of azobenzene due to the strong π - π interaction between the benzene rings and doxorubicin (DOX).^[20]

UV irradiation resulted in the *trans*-*cis* isomerization of azobenzene groups, as shown by the decrease in π - π^* absorption of the *trans* isomer at 330 nm and increase in the *n*- π^* band of the *cis* isomer at 450 nm (Figure S22, Supporting Information) in a time dependent manner. Furthermore, after X-ray irradiation, decreased absorption of the nanocapsules at 300 nm also indicated *trans*-*cis* photoisomerization in the bilayer membrane (Figure 3a), as well as high photoconversion capacity of the ZnS-A NPs. Meanwhile, the thickness of the PETAzo@ZnS-A

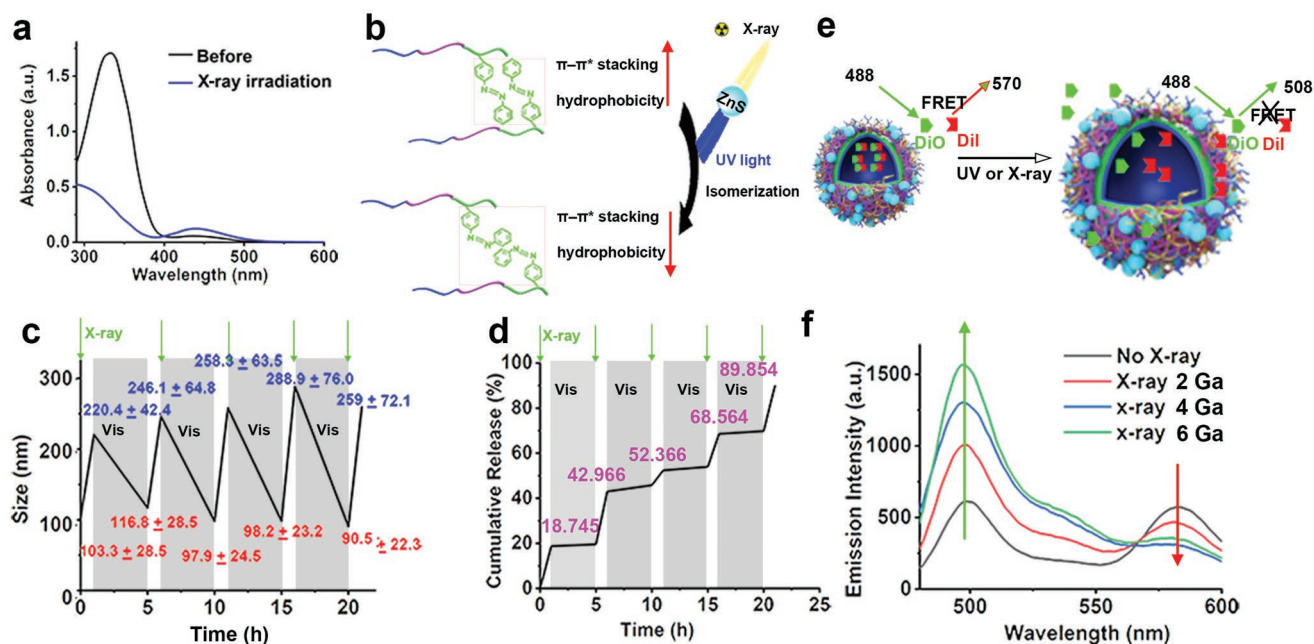


Figure 3. Characterization of PETAzo@ZnS-A nanocapsule during X-ray irradiation. a) UV-vis spectra of the nanocapsules before and after X-ray irradiation (6 Gy). b) Schematic illustration of transfer of X-rays to UV light by ZnS nanoparticles, further leading to realize X-ray-controlled reversible photochemical *trans-cis* isomerization of the azobenzene groups, subsequently decreasing $\pi-\pi^*$ stacking interaction and hydrophobicity of azobenzene. c) The size variation of PETAzo@ZnS-A nanocapsules after switched irradiation with X-rays and visible light for several cycles. d) Accumulated release profile of DOX from PETAzo@ZnS-A nanocapsules in the alternating presence of X-ray irradiation and visible light. e) Schematic illustration of FRET effect. f) Fluorescence spectra of PETAzo@ZnS-A nanocapsules at 4 h postirradiation with X-rays.

shell was about 35 nm. ZnS-A nanoparticles were compactly accumulated on the surface of nanocapsule (Figure 2c,e). The close packing of ZnS-A resulted in the aggregation effect with high conversion efficiency and avoided the emission effect of ZnS-A to be quenched by the environment. Without ZnS-A NPs on the surface of nanocapsules, the absorption of PETAzo nanocapsules at 300 and 450 nm was almost unchanged before or after X-ray irradiation (Figure S23, Supporting Information). In the meantime, PETAzo@ZnS-A nanocapsules before and after X-ray irradiation with different doses (2, 4, and 8 Gy) showed high photoconversion capacity of the ZnS-A NPs based on the variation of their UV-vis spectra (Figure S24, Supporting Information). To summarize, the X-rays were converted by the ZnS-A NPs to UV light which was absorbed by the azobenzene groups of PETAzo, resulting in reversible *trans-cis* isomerization, decreased $\pi-\pi^*$ stacking and hydrophobicity, increased membrane permeability to water soluble molecules, and swelled the nanocapsules (Figure 3b). Since *cis*-azobenzene is bulkier than the *trans* isoform, the *trans-cis* isomerization increases the core volume.^[21] As shown in Figure 3c, X-ray irradiation (6 Gy was used in all experiments unless otherwise stated) increased the size of PETAzo@ZnS-A nanocapsules from 100 to 200 nm, while visible light irradiation reverted the nanocapsules to the *trans* state with about 100 nm. The reversible photoisomerization of nanocapsules could be repeated at least four times, and enabled remotely controlled increase in permeability while maintaining structural integrity. The visual TEM images of the nanocapsules after single X-ray irradiation and four times alternating presence of X-ray irradiation and visible light indicated that the sizes of nanocapsules were increased after X-ray

irradiation (Figure S25, Supporting Information). In addition, X-ray irradiation released $\approx 18.7\%$ of the DOX from the nanocapsules within the first 1 h, and the cumulative amount of released DOX was $\approx 89.9\%$ (Figure 3d). The drug was able to passively diffuse across the nanocapsule bilayer membrane due to the concentration difference between the capsule interior and the outer medium, according to the Fickian diffusion release mechanism.^[22] The enhanced drug release under X-ray irradiation can be attributed to the increased permeability of nanocapsules after photoisomerization. The drug release of PETAzo@ZnS-A nanocapsules with alternating X-ray irradiation and visible light versus different single X-ray dose irradiation was evaluated. The drug release increased with the dose of X-ray irradiation from 2 to 8 Gy, indicating that the pulsatile drug release from PETAzo@ZnS-A nanocapsules could be controlled (Figure S26A, Supporting Information). After one round of X-ray irradiation, about 20% of DOX was released from the PETAzo@ZnS-A nanocapsules (Figure S26B, Supporting Information). The swollen PETAzo@ZnS-A nanocapsules would return to the original state after the X-ray irradiation was stopped, preventing further drug release. We employed the alternating cycles of X-ray and visible-light irradiation for controlled drug release. Unlike other polymer capsule membranes that cannot switch back to the initial state after releasing the encapsulated cargo, PETAzo@ZnS-A nanocapsules maintain their mechanical integrity after selective payload diffusion owing to this cross-linkage. The speed of drug release could be adjusted to the optimal content as needed. The pulsatile drug release under the alternating cycles of X-ray and visible light irradiation can satisfy the tumor cells with different drug sensitivities.

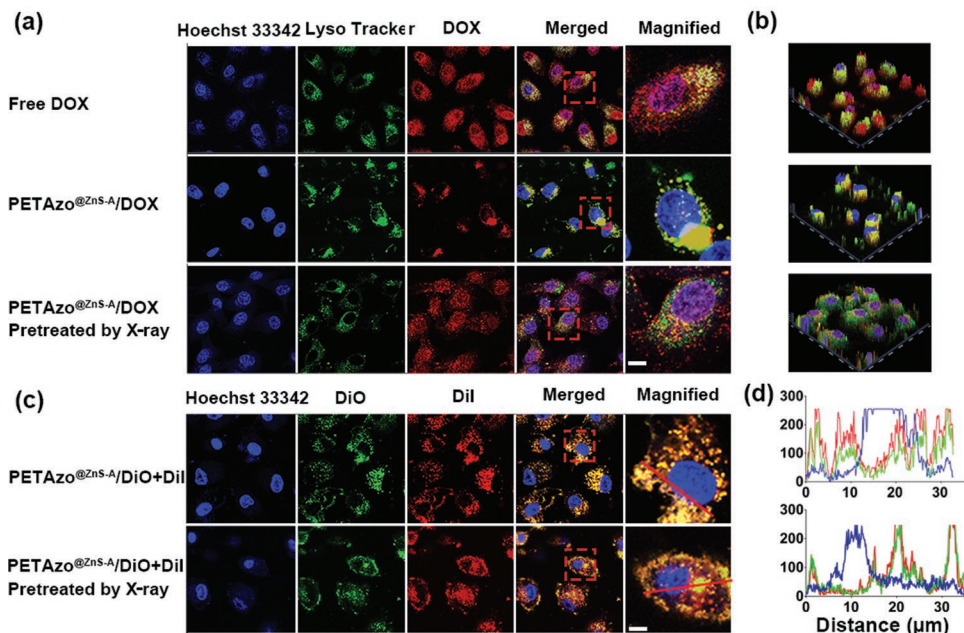


Figure 4. CLSM observations of U87MG cells treated with different formulations. a) Cellular internalization of free DOX and DOX-loaded PETAZo@ZnS-A nanocapsules (DOX: 2 $\mu\text{g mL}^{-1}$). Before incubation with cells, the DOX-loaded PETAZo@ZnS-A nanocapsules were pretreated by X-ray irradiation (6 Gy). b) 3D visualization of the coculture system by CLSM. c) Representative CLSM images of U87MG cells incubated with DiO and DiI-loaded PETAZo nanocapsules after 4 h incubation. Before incubation with cells, the DiO-loaded and DiI-loaded PETAZo nanocapsules were pretreated by X-ray irradiation (6 Gy). Scale bar: 20 μm (white, right). d) Line-scanning profiles of the fluorescence intensity in U87MG cells.

To examine the controlled permeability of the PETAZo@ZnS-A nanocapsules, they were loaded with a fluorescence resonance energy transfer (FRET) pair consisting of 3,3'-dioctadecyloxacarbocyanine perchlorate (DiO; donor, E_x/E_m 488/508 nm) and 1,1'-dioctadecyl-3,3,3',3'-tetramethylindocarbocyanine perchlorate (DiI; acceptor, E_x/E_m 508/570 nm). The characteristics of the FRET pair-loaded nanocapsules are summarized in Table S2 (Supporting Information). When the DiO/DiI-loaded PETAZo@ZnS-A nanocapsules were excited at 488 nm, the energy generated from DiO was transferred to DiI, resulting in emission at 570 nm. Upon release of the FRET pair from the nanocapsules, the distance between DiO and DiI increased (>10 nm), resulting in lower emission at 570 nm^[23] (Figure 3e). X-ray irradiation significantly increased the emission at 508 nm during a 4 h period (Figure 3f), indicating that the permeability of the nanocapsules could be controlled.

The intracellular trafficking of PETAZo@ZnS-A/DOX was tracked in U87MG cells using the Lyso Tracker Green DND-26, which stains the late endosomes and lysosomes. The U87MG cells were incubated with X-ray-irradiated or nonirradiated nanocapsules for 4 h. As shown in Figure 4a,b, nuclear localization of DOX was significantly higher with the irradiated PETAZo@ZnS-A/DOX nanocapsules due to faster drug release. As shown in Figure 4a, stronger fluorescence appeared both in the cytoplasm and nucleus of U87MG cells for free DOX than the DOX-loaded PETAZo@ZnS-A nanocapsules. It is known that DOX molecule can be internalized into tumor cells through a passive diffusion mechanism, while the DOX-loaded nanoparticles need to be endocytosed into the cells.^[24] The internalization of passive diffusion was much faster than that of endocytosis process.^[25] The FRET pair of DiO and DiI was also used to

evaluate the UV-triggered hydrophobic-to-hydrophilic transition of the nanocapsule membrane, since these probes bind to the phospholipid bilayer through hydrophobic interactions. As shown in Figure 4c,d, no FRET signals were emitted from the loaded PETAZo@ZnS-A/DOX nanocapsules in the absence of irradiation, whereas X-ray irradiation resulted in an emission peak at 508 nm due to photoisomerization of azobenzene and the subsequent changes as already described.

To further determine the efficacy of PETAZo@ZnS-A as a drug delivery system, the in vitro cytotoxicity of free DOX and PETAZo@ZnS-A/DOX were evaluated with or without X-ray irradiation. As shown in Figure 5a, the percentage of late apoptotic cells (Annexin V-FITC and 7AAD double stained) was 51.6% when treated with the irradiated PETAZo@ZnS-A/DOX, and only 25.6% following treatment with the nonirradiated nanocapsules. Consistent with the results, the IC₅₀ of PETAZo@ZnS-A/DOX in U87MG cells with or without X-ray irradiation were 1.389 and 4.198 $\mu\text{g mL}^{-1}$, respectively (Figure 5b,c). In vitro cytotoxicity evaluation of PETAZo@ZnS-A nanocapsules indicated that the free DOX has the best killing effect (Figure 5a). These results were consistent with the cellular uptake results (Figure 4). Caspase 3 initiates the apoptosis program following cleavage of procaspase 3.^[26] As shown in Figure 5d, cleaved caspase 3 levels were significantly higher in cells treated with the irradiated PETAZo@ZnS-A/DOX compared to other groups, in addition to 41% higher DNA fragmentation, as shown by TUNEL staining (Figure 5e). The greater cytotoxic effects of the PETAZo@ZnS-A/DOX nanocapsules upon X-ray irradiation were consistent with the controlled permeability and faster drug release as described.

We next evaluated the action of the nanocapsules in U87MG tumor-bearing mice, after ensuring absence of any hemolytic

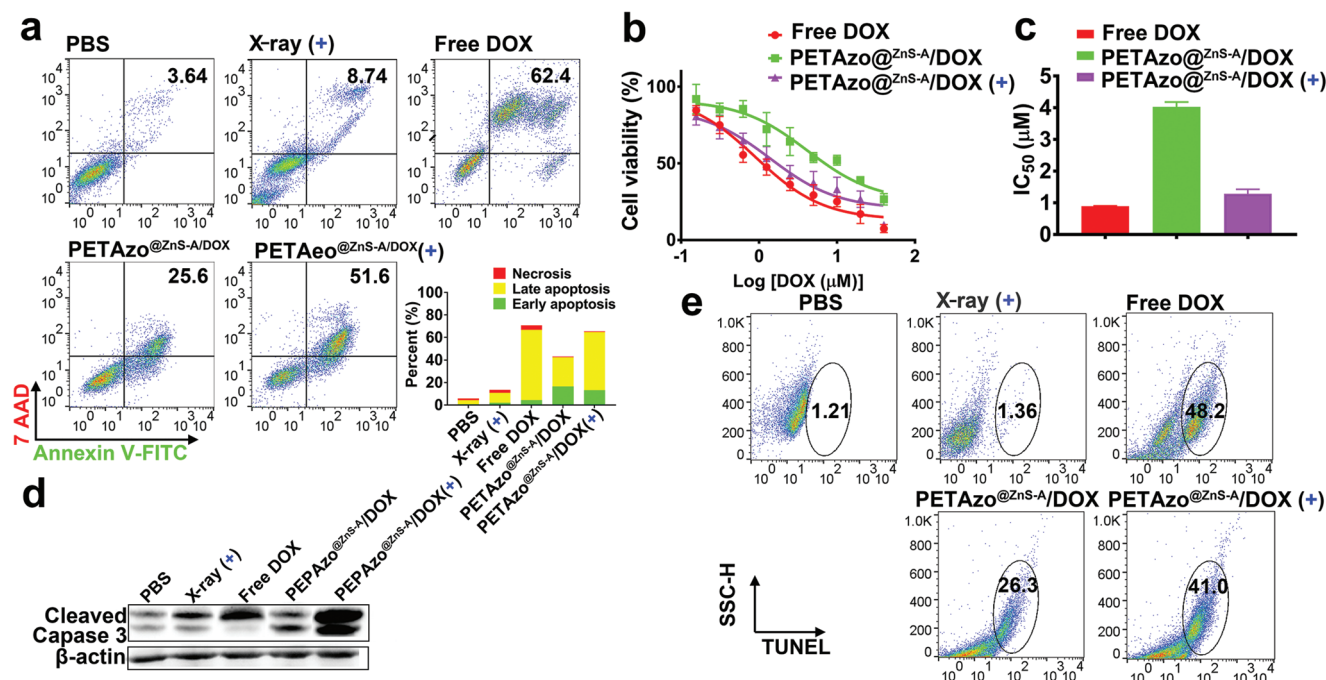


Figure 5. In vitro cytotoxicity evaluation of PETAZo@ZnS-A nanocapsules. a) Flow cytometry study of U87MG cells treated by PBS, X-rays (6 Gy), free DOX, PETAZo@ZnS-A nanocapsules, and PETAZo@ZnS-A nanocapsules with X-rays via Annexin V-FITC/7-AAD assays. b) The cell viability of U87MG cells after incubation with free DOX, PETAZo@ZnS-A nanocapsules, and PETAZo@ZnS-A nanocapsules with X-rays at various specified concentrations for 24 h. c) IC₅₀ (half inhibitory concentration) values of free DOX, DOX-loaded PETAZo@ZnS-A nanocapsules, and DOX-loaded PETAZo@ZnS-A nanocapsules with X-rays in U87MG cells. d) Western blot analysis of expression levels of the caspase family members after being treated by PBS, X-rays (6 Gy), free DOX, DOX-loaded PETAZo@ZnS-A nanocapsules, and DOX-loaded PETAZo@ZnS-A nanocapsules with X-rays. e) Flow cytometry study of cells treated by different samples for 24 h with and stained with TUNEL-FITC apoptosis kit. (+) represents that cells were applied with X-ray irradiation (6 Gy) before fixation.

effect of the PETAZo nanocapsules on the red blood cells (Figure S27, Supporting Information). The tumor-bearing mice were intravenously injected with indocyanine green (ICG)-loaded PETAZo or PETAZo@ZnS-A nanocapsules (ICG: 30 µg per 100 µL) and irradiated at 12 or 24 h postinjection (Figure 6a). As shown in Figure 6b,c, the mice injected with ICG-PETAZo@ZnS-A showed stronger fluorescence at the tumor site compared to those injected with ICG-PETAZo, indicating prolonged in vivo retention of the nanocapsules as a result of stabilizing nucleobase pairing interactions. Nanocarriers also accumulate in the tumor tissue by the enhanced permeability and retention (EPR) effect, for which their stability in blood circulation is a prerequisite.^[27] The stabilizing nucleobase pairing interactions also increased in situ accumulation of PETAZo@ZnS-A/ICG by preventing extravasation, which was validated by in vivo photoacoustic (PA) imaging (Figure 6b). The tumor-bearing mice were then injected with free DOX (5 mg kg⁻¹), PETAZo/DOX, and PETAZo@ZnS-A/DOX, and irradiated as above. While the plasma levels of DOX 36 h postinjection were similar across the three groups (Figure 6d), the total DOX amount in the tumor tissues was significantly higher in the PETAZo@ZnS-A compared to the PETAZo group (Figure 6e). The targeted accumulation of DOX is consistent with the excellent biostability of the nanocapsules. The biodistribution of PETAZo@ZnS-A and ZnS-A NPs in the tumor bearing nude mice was also evaluated by inductively coupled plasma mass spectrometric analysis of Zn in the different tissues (Figure 6f).

The maximum tolerated doses of PETAZo@ZnS-A/DOX and free DOX were also evaluated. As shown in Figure S28

(Supporting Information), DOX dosage between 5 and 15 mg kg⁻¹ via PETAZo@ZnS-A/DOX nanocapsules did not result in weight loss or death, whereas 10 mg kg⁻¹ free DOX was highly toxic to the mice. To determine the antitumor effects of PETAZo@ZnS-A/DOX nanocapsules, nude mice were injected with 1 × 10⁶ U87MG cells in 100 µL, and randomized one week later into the saline, saline + X-ray irradiation, free DOX (5 mg kg⁻¹ in all preparations), PETAZo@ZnS-A/DOX, and PETAZo@ZnS-A/DOX + X-ray irradiation groups, and treated accordingly (Figure 6g). As shown in Figure 6h, free DOX resulted in only 31.39% reduction in the tumor growth rate compared to the saline group, and the PETAZo@ZnS-A/DOX nanocapsules showed similarly weak antitumor effects without X-ray irradiation due to the inefficient drug release. Rapid clearance of free DOX in blood circulation is the main reason for its ineffectiveness in tumor suppression. By contrast, the blood circulation time of DOX-loaded nanoparticles was longer than that of free DOX. A similar result also can be found in some literatures.^[28] Therefore, compared to free DOX, DOX-loaded nanoparticles have a better antitumor effect. Upon X-ray irradiation, however, PETAZo@ZnS-A/DOX nanocapsules achieved 94.31% reduction in the tumor volume, without any detrimental effects on body weight and systemic health (Figure 6i). In addition, these tumor tissues showed increased levels of cleaved caspase-3^[29] and TUNEL-positive cells (Figure 6j,k), and significantly lower levels of the proliferation marker Ki-67.^[30] H&E staining showed large hypocellular and necrotic areas in the tumor xenografts of the PETAZo@ZnS-A/DOX + X-ray irradiation group, without any pathological changes in the heart, liver,

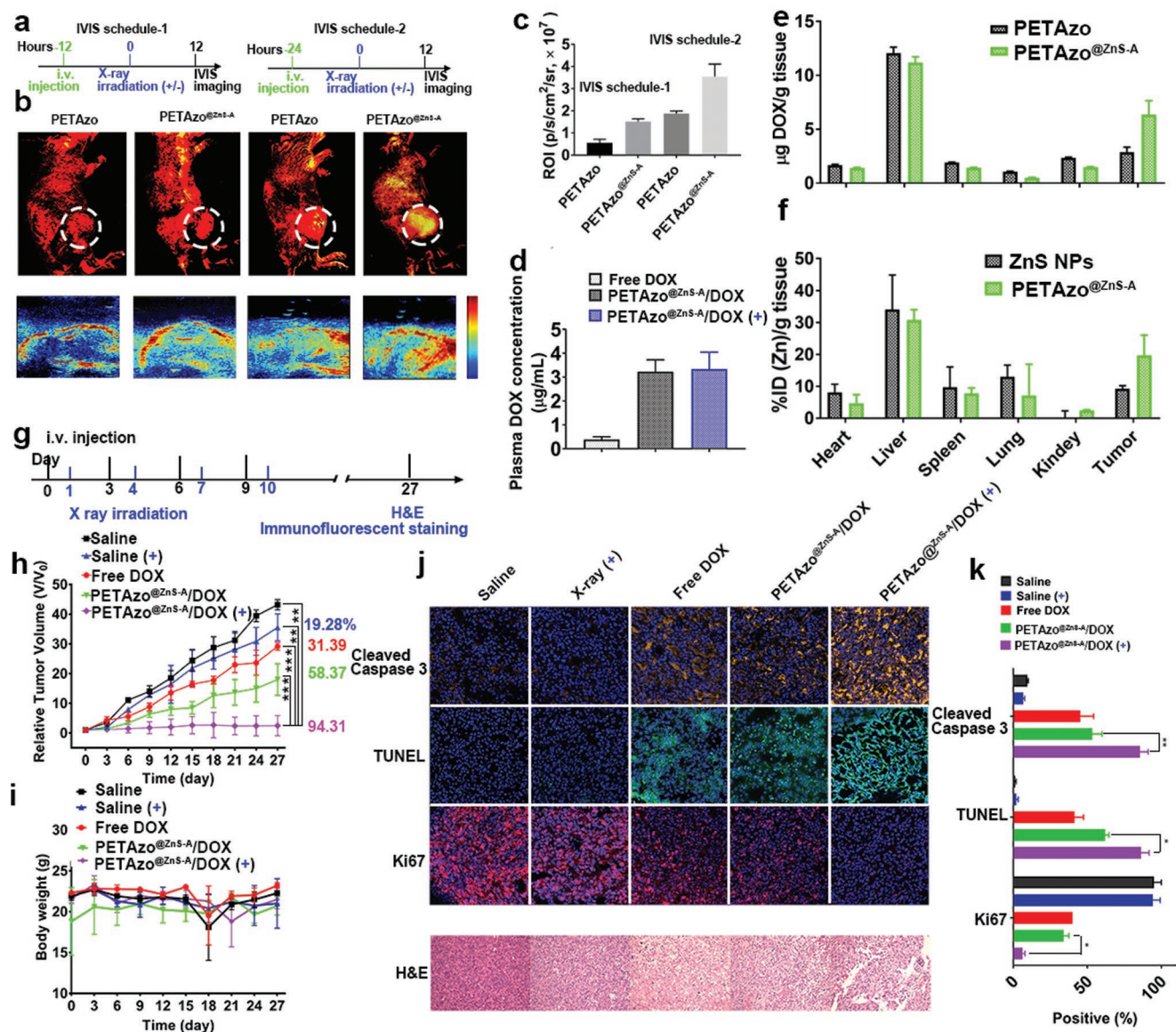


Figure 6. In vivo imaging and therapeutic efficacy of PETAzo@ZnS-A nanocapsules. a) Schematic representation of the manipulation schedule. b) In vivo fluorescence imaging (top) and PA imaging (bottom) of the U87MG tumor-bearing nude mice after intravenous injection of ICG-loaded PETAzo or PETAzo@ZnS-A nanocapsules. c) The quantitative region-of-interest (ROI) of fluorescent signals of the tumor. d) The plasma concentration of DOX at 36 h postinjection of the DOX-loaded PETAzo@ZnS-A nanocapsules according to the manipulation schedule. e) Biodistribution of DOX in different organs and tissues after intravenous administration of DOX-loaded PETAzo@ZnS-A nanocapsules. f) Biodistribution of PETAzo@ZnS-A nanocapsules in different organs and tissues at 36 h postinjection of the DOX-loaded nanocapsules. g) Schematic representation of the in vivo therapy schedule. h) The relative tumor volumes after different treatments. i) Body weight variation of mice in different treatment group. j) Immunofluorescent and histology staining of the tumor tissue. k) Quantification of (j), data are expressed as the mean ± SD from at least three independent experiments. **P* < 0.05; ***P* < 0.01; ****P* < 0.001. All images are 10× magnification.

spleen, lung, and kidney (Figure S29, Supporting Information), indicating the biosafety of these nanocapsules.

In conclusion, we have successfully developed X-ray-responsive PETAzo@ZnS-A nanocapsules with reversible and controllable permeability, which achieved efficient and targeted drug release in vivo upon X-ray irradiation, resulting in effective tumor clearance. ZnS NPs can efficiently convert X-rays into UV-vis light to induce the isomerization of azobenzene groups, subsequently decreasing π - π^* stacking interaction and hydrophobicity of azobenzene, inducing the swelling of nanocapsules,

and enhancing the bilayer permeability to realize precise drug delivery. In comparison with the conventional method that regulates nanostructure permeability by disrupting the structure of nanocapsules and is a nonreversible process, PETAzo@ZnS-A nanocapsules with remotely controlled bilayer permeability can realize the tunable permeability while maintaining the structural integrity. In vitro and in vivo results indicated that the X-ray-triggered nanocapsule could dominate the drug release behavior to satisfy the complicated sensitivities of different tumor cells and different patients to realize precise cancer therapy.

Supporting Information

Supporting Information is available from the Wiley Online Library or from the author.

Acknowledgements

This research was supported by National Natural Science Foundation of China (NSFC) projects (Grant number: 201874024), and the intramural research program of the National Institute of Biomedical Imaging and Bioengineering (NIBIB), National Institutes of Health (NIH). The U87MG human glioblastoma cell line was obtained from the American Type Culture Collection. All the experimental procedures involving animals were conducted following a protocol approved by the animal care and use committee (ACUC) of the National Institutes of Health Clinical Center (NIHCC).

Conflict of Interest

The authors declare no conflict of interest.

Keywords

azobenzene, controlled drug release, nucleobase pairing, permeability, X-rays

Received: May 30, 2019

Revised: July 13, 2019

Published online: August 5, 2019

- [1] a) M. Kathan, S. Hecht, *Chem. Soc. Rev.* **2017**, *46*, 5536; b) R. Merindol, A. Walther, *Chem. Soc. Rev.* **2017**, *46*, 5588; c) H. Che, S. Cao, J. C. M. van Hest, *J. Am. Chem. Soc.* **2018**, *140*, 5356; d) Y. Zhang, S. Tsitkov, H. Hess, *Nat. Catal.* **2018**, *1*, 276.
- [2] a) U. Kauscher, M. N. Holme, M. Björnalm, M. M. Stevens, *Adv. Drug Delivery Rev.* **2019**, *138*, 259; b) T. Heuser, E. Weyandt, A. Walther, *Angew. Chem., Int. Ed.* **2015**, *54*, 13258; c) T. Heuser, R. Merindol, S. Loescher, A. Klaus, A. Walther, *Adv. Mater.* **2017**, *29*, 1606842; d) Y. Okamoto, T. R. Ward, *Angew. Chem., Int. Ed.* **2017**, *56*, 10156.
- [3] H. Deng, X. Zhao, L. Deng, J. Liu, A. Dong, *J. Controlled Release* **2017**, *255*, 142.
- [4] L. Wang, Q. Li, *Chem. Soc. Rev.* **2018**, *47*, 1044.
- [5] a) A. Johnston, C. Cortez, A. Angelatos, F. Caruso, *Curr. Opin. Colloid Interface Sci.* **2006**, *11*, 203; b) J. Qi, X. Lai, J. Wang, H. Tang, H. Ren, Y. Yang, Q. Jin, L. Zhang, R. Yu, G. Ma, Z. Su, H. Zhao, D. Wang, *Chem. Soc. Rev.* **2015**, *44*, 6749; c) J. Cui, J. Richardson, M. Bjornmalm, M. Faria, F. Caruso, *Acc. Chem. Res.* **2016**, *49*, 1139.
- [6] G. Ragazzon, M. Baroncini, S. Silvi, M. Venturi, A. Credi, *Nat. Nanotechnol.* **2015**, *10*, 70.
- [7] a) M. Baroncini, S. d'Agostino, G. Bergamini, P. Ceroni, A. Comotti, P. Sozzani, I. Bassanetti, F. Grepioni, T. M. Hernandez, S. Silvi, M. Venturi, A. Credi, *Nat. Chem.* **2015**, *7*, 634; b) H. Zhou, C. Xue, P. Weis, Y. Suzuki, S. Huang, K. Koynov, G. K. Auernhammer, R. Berger, H.-J. Butt, S. Wu, *Nat. Chem.* **2017**, *9*, 145.
- [8] A. Kravchenko, A. Shevchenko, V. Ovchinnikov, A. Priimagi, M. Kaivola, *Adv. Mater.* **2011**, *23*, 4174.
- [9] S. Venkataramani, U. Jana, M. Dommaschk, F. D. Sönnichsen, F. Tuzcek, R. Herges, *Science* **2011**, *331*, 445.
- [10] a) F.-K. Bruder, R. Hagen, T. Rölle, M.-S. Weiser, T. Fäcke, *Angew. Chem., Int. Ed.* **2011**, *50*, 4552; b) T. J. Kucharski, N. Ferralis, A. M. Kolpak, J. O. Zheng, D. G. Nocera, J. C. Grossman, *Nat. Chem.* **2014**, *6*, 441.
- [11] A. H. Gelebart, D. Jan Mulder, M. Varga, A. Konya, G. Vantomme, E. W. Meijer, R. L. B. Selinger, D. J. Broer, *Nature* **2017**, *546*, 632.
- [12] a) S. Wu, H.-J. Butt, *Adv. Mater.* **2016**, *28*, 1208; b) Z. Li, E. Ye, David, R. Lakshminarayanan, X. J. Loh, *Small* **2016**, *12*, 4782.
- [13] a) K. Szaciłowski, W. Macyk, A. Drzewiecka-Matuszek, M. Brindell, G. Stochel, *Chem. Rev.* **2005**, *105*, 2647; b) R. Cai, Y. Kubota, T. Shuin, H. Sakai, K. Hashimoto, A. Fujishima, *Cancer Res.* **1992**, *52*, 2346; c) B. Yan, J.-C. Boyer, D. Habault, N. R. Branda, S. Zhao, *J. Am. Chem. Soc.* **2012**, *134*, 16558.
- [14] a) S. H. Yun, S. J. J. Kwok, *Nat. Biomed. Eng.* **2017**, *1*, 0008; b) G. Jalani, V. Tam, F. Vetrone, M. Cerruti, *J. Am. Chem. Soc.* **2018**, *140*, 10923.
- [15] Z. Du, X. Zhang, Z. Guo, J. Xie, X. Dong, S. Zhu, J. Du, Z. Gu, Y. Zhao, *Adv. Mater.* **2018**, *30*, 1804046.
- [16] a) C. Yao, P. Wang, X. Li, X. Hu, J. Hou, L. Wang, F. Zhang, *Adv. Mater.* **2016**, *28*, 9341; b) T. Zhao, P. Wang, Q. Li, A. A. Al-Khalaf, W. N. Hozzein, F. Zhang, X. Li, D. Zhao, *Angew. Chem.* **2018**, *130*, 2641.
- [17] M. Zhao, B. Li, P. Wang, L. Lu, Z. Zhang, L. Liu, S. Wang, D. Li, R. Wang, F. Zhang, *Adv. Mater.* **2018**, *30*, 1804982.
- [18] X. Zhao, H. Deng, H. Feng, J. Zhang, A. Dong, L. Deng, *Macromol. Chem. Phys.* **2016**, *217*, 2611.
- [19] a) L. Guo, S. Chen, L. Chen, *Colloid Polym. Sci.* **2007**, *285*, 1593; b) C. Lü, J. Gao, Y. Fu, Y. Du, Y. Shi, Z. Su, *Adv. Funct. Mater.* **2008**, *18*, 3070.
- [20] J. Zhao, H. Wang, J. Liu, L. Deng, J. Liu, A. Dong, J. Zhang, *Biomacromolecules* **2013**, *14*, 3973.
- [21] a) Q. Ye, M. Huo, M. Zeng, L. Liu, L. Peng, X. Wang, J. Yuan, *Macromolecules* **2018**, *51*, 3308; b) T. Hamada, Y. T. Sato, K. Yoshikawa, T. Nagasaki, *Langmuir* **2005**, *21*, 7626.
- [22] a) S. Yan, J. Zhu, Z. Wang, J. Yin, Y. Zheng, X. Chen, *Eur. J. Pharm. Biopharm.* **2011**, *78*, 336; b) S. Shu, C. Sun, X. Zhang, Z. Wu, Z. Wang, C. Li, *Acta Biomater.* **2010**, *6*, 210.
- [23] a) H. Deng, X. Zhao, J. Liu, J. Zhang, L. Deng, J. Liu, A. Dong, *Nanoscale* **2016**, *8*, 1437; b) S. Jiwanpanich, J.-H. Ryu, S. Bickerton, S. Thayumanavan, *J. Am. Chem. Soc.* **2010**, *132*, 10683; c) H. Chen, S. Kim, L. Li, S. Wang, K. Park, J.-X. Cheng, *Proc. Natl. Acad. Sci. USA* **2008**, *105*, 6596.
- [24] L. Pan, Q. He, J. Liu, Y. Chen, M. Ma, L. Zhang, J. Shi, *J. Am. Chem. Soc.* **2012**, *134*, 5722;
- [25] H. Zheng, S. Li, Y. Pu, Y. Lai, B. He, Z. Gu, *Eur. J. Pharm. Biopharm.* **2014**, *87*, 454.
- [26] a) S. Meynier, F. Rieux-Laucat, *Immunol. Rev.* **2019**, *287*, 50; b) R. Singh, A. Letai, K. Sarosiek, *Nat. Rev. Mol. Cell Biol.* **2019**, *20*, 175; c) L. Galluzzi, A. López-Soto, S. Kumar, G. Kroemer, *Immunity* **2016**, *44*, 221.
- [27] H. Deng, Y. Zhang, X. Wang, J. Zhang, Y. Cao, J. Liu, J. Liu, L. Deng, A. Dong, *Acta Biomater.* **2015**, *11*, 126.
- [28] a) A. Jain, A. Agarwal, S. Majumder, N. Lariya, A. Khaya, H. Agrawal, S. Majumdar, G. P. Agrawal, *J. Controlled Release* **2010**, *148*, 359; b) H.-J. Cho, I.-S. Yoon, H. Y. Yoon, H. Koo, Y.-J. Jin, S.-H. Ko, J.-S. Shim, K. Kim, I. C. Kwon, D.-D. Kim, *Biomaterials* **2012**, *33*, 1190; c) J. Fu, L. Liang, L. Qiu, *Adv. Funct. Mater.* **2017**, *27*, 1604981.
- [29] a) C. Rogers, T. Fernandes-Alnemri, L. Mayes, D. Alnemri, G. Cingolani, E. S. Alnemri, *Nat. Commun.* **2017**, *8*, 14128; b) B. Li, P. Hong, C.-C. Zheng, W. Dai, W.-Y. Chen, Q.-S. Yang, L. Han, S. W. Tsao, K. T. Chan, N. P. Y. Lee, S. Law, L. Y. Xu, E. M. Li, K. W. Chan, Y. R. Qin, X. Y. Guan, M. L. Lung, Q.-Y. He, W. W. Xu, A. L. Cheung, *Theranostics* **2019**, *9*, 1599; c) T. Ishii, H. Hayakawa, T. Igawa, T. Sekiguchi, M. Sekiguchi, *Proc. Natl. Acad. Sci. USA* **2018**, *115*, 6715.
- [30] W. Xue, L. Zender, C. Miething, R. A. Dickins, E. Hernando, V. Krizhanovskiy, C. Cordon-Cardo, S. W. Lowe, *Nature* **2007**, *445*, 656.